



HAL
open science

Study of the interaction of a short fatigue crack with grain boundaries in a cast Al alloy using X-ray microtomography

Wolfgang Ludwig, Jean-Yves Buffière, Stéphane Savelli, Peter Cloetens

► To cite this version:

Wolfgang Ludwig, Jean-Yves Buffière, Stéphane Savelli, Peter Cloetens. Study of the interaction of a short fatigue crack with grain boundaries in a cast Al alloy using X-ray microtomography. *Acta Materialia*, 2003, 51 (3), pp.585-598. 10.1016/S1359-6454(02)00320-8 . hal-00475154

HAL Id: hal-00475154

<https://hal.science/hal-00475154>

Submitted on 17 May 2023

HAL is a multi-disciplinary open access archive for the deposit and dissemination of scientific research documents, whether they are published or not. The documents may come from teaching and research institutions in France or abroad, or from public or private research centers.

L'archive ouverte pluridisciplinaire **HAL**, est destinée au dépôt et à la diffusion de documents scientifiques de niveau recherche, publiés ou non, émanant des établissements d'enseignement et de recherche français ou étrangers, des laboratoires publics ou privés.



Distributed under a Creative Commons Attribution - NonCommercial 4.0 International License

Study of the interaction of a short fatigue crack with grain boundaries in a cast Al alloy using X-ray microtomography

W. Ludwig ^{a,* 1}, J-Y. Buffière ^c, S. Savelli ^b, P. Cloetens ^a

^a *European Synchrotron Radiation Facility, BP220, 38043 Grenoble, France*

^b *Pechiney Centre de Recherches de Voreppe, BP27, 38341 Voreppe Cedex, France*

^c *Lab. GEMPPM, INSA-Lyon, 69621 Villeurbanne Cedex, France*

Synchrotron Radiation X-ray microtomography is used to visualize and analyze simultaneously the three-dimensional shape of crystallographic grains containing a short fatigue crack in a cast Al alloy. The visualization of the grains is based on the decoration of Al grain boundaries by liquid Ga which serves as a selective contrast agent. The intricate three-dimensional shape of the fatigue crack, as well as the crack stops observed on the sample surface, are correlated to the grain structure of the material. Complementary measurements of the grain orientation on the sample surface by electron backscattering diffraction (EBSD) allow us to discuss and interpret the observations in terms of possible crack propagation mechanisms.

Résumé

La micro-tomographie utilisant le rayonnement X synchrotron est utilisée pour visualiser et analyser simultanément la forme tridimensionnelle de grains cristallographiques contenant une fissure courte de fatigue dans un alliage d'aluminium de moulage. La visualisation des grains repose sur la décoration des joints de grains de l'alliage d'aluminium par le gallium liquide qui sert de marqueur sélectif. La forme compliquée de la fissure de fatigue au sein du matériau ainsi que les arrêts de la fissure observées à la surface du matériau apparaissent corrélés à la structure des grains sous la surface de l'échantillon. La détermination de l'orientation cristallographique des grains par diffraction des électrons rétro-diffusés (EBSD) permet de discuter et interpréter ces résultats en terme de mécanismes de propagation des fissures.

¹ Current address: Lab GEMPPM, INSA-Lyon, 69621 Villeurbanne Cedex, France.

* Corresponding author. Tel.: +33 4 72 43 89 90; fax: +33 4 72 43 85 39.

E-mail address: ludwig@insa-lyon.fr (W. Ludwig).

Zusammenfassung

Mit Hilfe von Synchrotronstrahlung-Röntgenmikrotomographie gelingt es die Kornstruktur einer Aluminium Guss-Legierung in der unmittelbaren Nachbarschaft eines Ermüdungsrissses dreidimensional abzubilden. Die Abbildung der Kornstruktur beruht auf der selektiven Benetzung der Aluminium Korngrenzen mit flüssigem Gallium, welches als Kontrastmittel verwendet wird. Die komplizierte Form des Ermüdungsrissses im Inneren der Probe, sowie die an der Probenoberfläche beobachteten Verzögerungen in der Rissausbreitung können mit der Kornstruktur in Verbindung gebracht werden. Die zusätzliche Analyse der Kornorientierungen mit Hilfe der Rückstreuungselektronenbeugung (EBSD), ermöglicht die Diskussion und Interpretation der Ergebnisse hinsichtlich verschiedener Rissausbreitungsmechanismen.

Keywords: Short fatigue crack; Microtomography; Grain boundary wetting; Gallium; PACS:

1. Introduction

The Paris law which relates the growth rate da/dN of a fatigue crack to the stress intensity factor ΔK is extensively used to predict the fatigue life of engineering components. However, in many engineering metallic alloys, it has been observed that small cracks (with a size typically smaller than a few grains [1]), do not show a “regular” growth with ΔK (as described by the Paris law) but some accelerations and retardations due to their interactions with microstructural features [2]. If neglected, this so called short crack phenomenon can lead to a serious over estimation of the fatigue life [3]. It is therefore a crucial problem to tackle. Among all the microstructural features which can alter the propagation of short cracks, grain boundaries have been observed to play a key role [2,4–9]. However, the experimental study of the interaction of short fatigue cracks with grain boundaries is greatly complicated by the fact that it is a three dimensional problem. A few studies have shown that the abnormal growth of fatigue cracks as observed from the surface of a sample can be accounted for by the presence of some sub surface microstructural features [10,11]. Those studies are based on serial polishing and optical observations of fatigue samples, a quite tedious and destructive experimental technique which strongly limits the number of observations and which is not free of artifacts (e.g. crack blurring in ductile materials). In the last five years, however, the availability of new powerful synchrotron X-ray sources has opened the way for three dimensional (3D) imaging of the interior

of materials through the use of high resolution microtomography. This technique which gives direct images of internal defects in the micrometer range has been used, for example, to study fatigue crack closure in Al-Li alloys [12] but also damage *development* in various heterogeneous materials by repeated inspection of the specimens at different deformation stages [13–18]. The use of coherent X-rays has also been shown to improve the detection of cracks and microstructural features in strained metal matrix composites [19].

In this work, high resolution microtomography has been used to visualize *simultaneously* the 3D shape of a short fatigue crack in a cast aluminium alloy and of the surrounding grains. The grain visualisation is achieved by applying liquid Ga to the sample surface. Ga penetrates along the grain boundaries into the bulk of the material and leads to the formation of microscopic grain boundary wetting layers which can be detected by X-ray absorption imaging [20]. The 3D images obtained with this technique clearly show that the surface growth of short cracks is strongly correlated to sub surface microstructural features. Besides, the analysis of the crack shape with respect to the local grain boundaries also reveals the importance of the crack-plane tilt and twist for the propagation rate of stage I cracks as suggested by other authors [21].

2. Experimental methods

A model AS7G03 cast alloy containing artificial pores has been used in this study. A complete

description of the microstructure and fatigue deformation mechanisms of this material can be found elsewhere [22,14], only the main details are given in what follows. The alloy, which chemical composition is given in Table 1, was chill mould cast in a silicon carbide mould. The artificial pores were obtained by introducing at 1093 K a mixture of hydrogen (H_2) and argon (Ar) gases in the liquid metal through a propeller. After cooling, the alloy was solution treated during 10 h at 813 K, quenched in cold water, and aged during 6 h at 433 K (T6 heat treatment). The resulting microstructure is shown in Fig. 2a and b. It consists in large grains with an average size of 300 μm (2D measurements), containing a mixture of primary α aluminium dendrites separated by the eutectic phase containing small silicon particles with an average size of 3 μm . The fatigue behaviour of the material has been studied during constant stress amplitude tests ($120 \leq \Delta\sigma \leq 240$ MPa) at room temperature in air with a load ratio $R = 0.1$ and a frequency of 10 Hz.

One fatigue sample has been prepared for tomographic investigation according to the sequence described below:

1. An interrupted fatigue test with a stress amplitude $\Delta\sigma = 160$ MPa was carried out and the surface growth of a crack initiated on one sample's corner was monitored each 25.000 cycles during 375.000 cycles by optical microscopy.
2. After the test, the grain orientation at the surface around the crack was determined by the use of electron backscattering diffraction (EBSD, surface XZ defined in Fig. 1).
3. One needle shape tomography sample with a square cross section of 0.7×0.7 mm² and a length of 5 mm was carefully cut with a wire saw around the fatigue crack (see Fig. 1).

Table 1
Chemical composition (mass %) of the studied model cast Al alloy.

Al	Si	Fe	Mg	Ti	Sb	Cr	rest
92.5	6.6–7	0.09– 0.14	0.29– 0.34	0.11– 0.14	0.12– 0.14	0.2	≤ 0.01

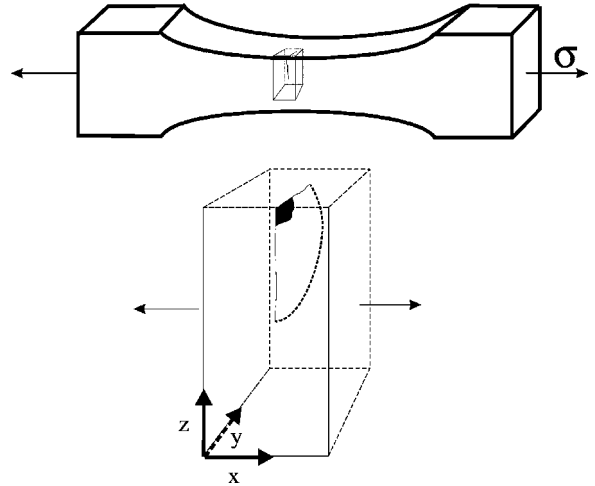


Fig. 1. Schematic representation of the geometry of the fatigue sample. The indicated small parallelepiped (0.7×0.7×5 mm) containing the short fatigue crack was wire-cut from the original specimen and characterized by synchrotron radiation microtomography.

4. A first tomographic scan was performed in order to study the 3D shape of the crack in the bulk of the sample.
5. The sample was then exposed to liquid gallium and annealed for 1 h at 100 °C.
6. A second tomographic scan, revealing the grain boundary structure was recorded.
7. The (now fragile) sample has been embedded into epoxy resin, cut along the XY plane and polished in order to determine the crystallographic orientation of sub-surface grains via EBSD measurements.

2.1. Microtomographic imaging

The tomographic imaging experiments were carried out at the ID19 beamline of the European Synchrotron Radiation Facility (ESRF), Grenoble. The dedicated microtomographic set-up consists of a precision mechanic sample stage combined with a fast, high resolution detector system. The detector system itself is based on a 26 μm thick transparent fluorescent screen (LAG: Eu) [23] which transforms the X-rays into visible light and microscope optics to project the image on the Peltier cooled 1024² CCD camera. The latter has a dynamic range of 13 bits, fast readout (0.06

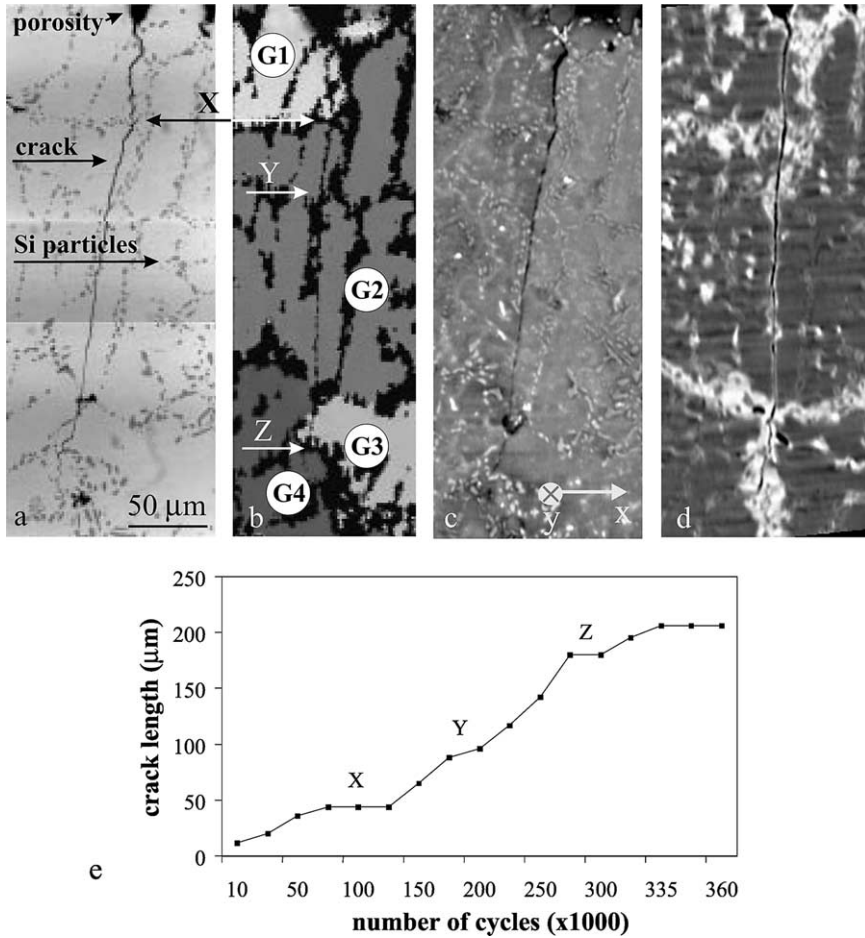


Fig. 2. a) Optical micrograph of the fatigue crack at the sample surface b) EBSD mapping of the same zone c) tomographic reconstruction of the sample surface before application of Gallium (energy: 15 keV, distance: 5 mm) d) tomographic reconstruction after application of Gallium e) plot of crack length versus number of cycles as observed by optical microscopy during the interrupted fatigue test.

s/frame) and a low dark current (3 e-/s) [24]. The spatial resolution was determined with the knife-edge method to be 1.7 μm (full width half maximum of the line spread function) for the optical magnification used in our experiments (effective pixel size: 0.95 μm). The need for ultimate spatial resolution in order to resolve cracks with micron and sub-micron widths restricts the field of view and consequently the sample cross-

section² to approximately 1 mm. In order to obtain high quality 3D images the incoming 'white' synchrotron radiation was monochromatized to 15 keV using a synthetic Rb-B₄C multilayer with large energy bandwidth ($\Delta\lambda/\lambda = 2 \times 10^{-2}$) [25].

² For tomographic reconstruction the sample has to fit laterally entirely into the field of view.

Typical scan times (1000 projections over 180 degrees, 13 bit dynamic range, 1 μm pixelsize) are of the order of 20 min. After some basic image processing (subtraction of dark current, flat field correction), the 3D distribution of the linear attenuation coefficient μ is calculated using the filtered backprojection algorithm [26]. The resulting three-dimensional dataset consists in a set of isotropic voxels ³ and can be visualised and analysed using dedicated 3D image processing software packages.

It should be noted that the coherence properties of third generation synchrotron beams can be used to perform phase sensitive X-ray imaging. By increasing the sample to detector distance to a few centimeters, sample defects and heterogeneities give rise to pronounced interference effects (Fresnel diffraction, in-line holography). The use of this phenomenon leads to a contrast enhancement which improves the sensitivity of the tomography technique for detecting cracks in materials by at least one order of magnitude [19]. Part of the work presented in this article is based on this phase sensitive imaging technique.

2.2. Grain boundary imaging

Currently only a few experimental techniques allow us to characterize the three-dimensional arrangement of grains in the bulk of a polycrystalline material: serial sectioning, either mechanically or by the focussed ion beam technique (limited to grain sizes below 20 μm [27]), and X-ray tracking [28,29]. The sectioning techniques have the disadvantage of being extremely laborious and destructive. X-ray tracking on the other hand is a non-destructive technique based on Laue diffraction and provides the shape and crystallographic orientation of the individual grains in the bulk of a polycrystalline material. However, the current spatial resolution of the latter technique does not exceed 20–40 μm and it does not allow to detect the existence of cracks.

Due to their small lateral width, natural grain

boundaries can not be detected by the change in X-ray attenuation. However, for the case of Al alloys we recently pointed out the possibility to visualize the 3D grain structure by using liquid Ga as a contrast agent for X-ray absorption tomography [20]. When applied to the surface of a polycrystalline Al sample, liquid Ga ($T_m = 29.7\text{ }^\circ\text{C}$) penetrates rapidly ($\cong 10\text{ }\mu\text{m/s}$) [30] along the grain boundaries where it tends to form liquid layers of up to one micrometer thickness. Due to the fact that Ga has a considerably higher X-ray attenuation coefficient than Al, these layers can be easily detected by means of high resolution absorption microtomography (see Fig. 5). In order to improve the visibility of the wetting layer, the sample is annealed for about one hour at 100 $^\circ\text{C}$ before the acquisition of the tomographic dataset. This annealing leads to volume diffusion of Ga into the neighboring grains and increases the width and the continuity of the wetting layers in the tomographic reconstruction. Note that only grain boundaries which fulfill the wetting condition $v_{gb} > 2v_{sl}$, where v_{gb} and v_{sl} denote the grain boundary and solid-liquid interface tensions respectively, are prone to penetration. Special grain boundaries and low angle grain boundaries are known to have lower surface tensions and might therefore not be detected by this technique. It should also be noted, that the penetration process leads to the complete loss of the mechanical strength of the material (grain decohesion by the liquid metal) and this technique has, therefore, to be considered as a destructive one which can only be applied at the end of the fatigue experiment.

In order to be able to characterize and visualize the individual grains in a convenient way, the tomographic dataset has to be segmented and labeled in order to extract the grain structure. The transformation of the tomographic raw data, containing the three-dimensional arrangement of the grain boundaries, into its segmented representation is shown in Fig. 5. All voxels belonging to the same crystallographic grain (a grain is defined by the closed grain boundary surface which delimits it) have been attributed the same colour label. Despite its apparent simplicity for the human eye, the computer implementation of this procedure is not straightforward and requires a considerable

³ 3D equivalent to the 2D pixel; represents the smallest digital volume of the material from which the X-ray attenuation is determined.

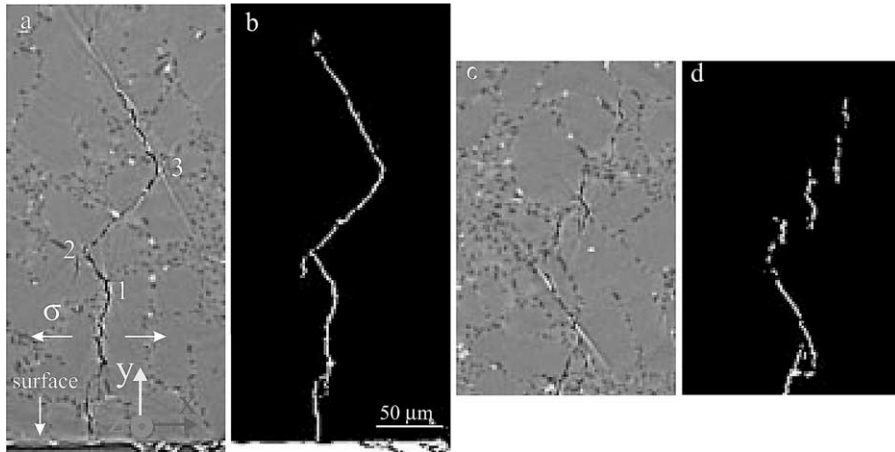


Fig. 3. a,c): Tomographic slices perpendicular to the surface of observation revealing the complicated morphology of the crack in the bulk of the sample (energy: 15 keV, distance 42 mm). b,d): corresponding slices after segmentation by 3D morphologic reconstruction.

amount of image processing. In a first step the data set is binarised by applying an intensity threshold. In order to keep all voxels belonging to the grain boundaries, this threshold has to be chosen rather low and results in a relatively noisy representation of the grain boundary structure. This binarised dataset in turn has to be cleaned by a series of morphological filter operations before it can be passed to the actual segmentation routine (3D watershed algorithm) [31,32]. The segmented volume is finally labeled and can now be visualized with adapted volume rendering software packages.

3. Results

3.1. Observations of the crack at the surface of the sample: the validation of the method

The results of the crack propagation experiment are summarized in Fig. 2. The optical micrograph on the left side (Fig. 2a) shows the crack path at the sample surface (plane XZ on Fig. 1). As already observed for other samples of this material, crack initiation occurred on a Si particle/matrix interface at the immediate vicinity of a pore. Fig. 2b) shows an EBSD map of the same zone and reveals the position and orientation of the grains along the crack path. The crack, as well as the silicon rich particles cannot be indexed in the map and appear

as black points. Note, that the Si particles are not only located at the grain boundaries, but also inside grains. The crack growth chronology, as determined from surface observations, is reported in Fig. 2e. From this figure, it can be seen that the crack stopped at the surface for $\cong 50000$ and $\cong 25000$ cycles on two grain boundaries visible on the EBSD surface map (points 'X' and 'Z'). A shorter arrest of the crack ($\cong 20000$ cycles) was also observed (point 'Y') but does not seem to be correlated with the presence of a grain boundary at the surface. The tomographic reconstructions of the sample surface before and after application of gallium are shown on Fig. 2c and d respectively. Although the presence of the sample surface deteriorates the quality of those images slightly ⁴ it appears that the crack shape observed on reconstructed images is very close to that observed by optical microscopy. The white contrast in Fig. 2d is due to the enhanced absorption caused by the presence of liquid Ga which has penetrated the grain boundaries [20]. Note that the gallium also wets the crack surface. ⁵ The rather large width of

⁴ On reconstructed slices in the bulk of the material, individual Si particles can be more clearly visualized, see for example Fig. 3a.

⁵ It is always possible, however, to distinguish the crack from a grain boundary by comparing with the tomographic scan obtained before the application of gallium.

the Ga rich zone (about 10 μm) is a result of the volume diffusion from the wetted grain boundary into the adjacent grains during the mentioned heat treatment at 100°C. Again, a good match is obtained between the reconstructed gallium layers and the grain boundaries as observed by EBSD (Fig. 2b). From those comparisons it is concluded that both the crack and the grain shapes in the interior of the sample can be studied with a good accuracy from the tomographic images.

3.2. Observations of the crack in the bulk of the sample

The crack path in the interior of the sample is strikingly more complex than the relatively linear propagation observed at the surface. This is illustrated on Fig. 3a and c which show two tomographic slices parallel to the XY plane defined in Fig. 1. Three marked changes in the direction of the crack can be seen on Fig. 3a. In addition, when going further in the material along the same direction, small crack segments appear, apparently disconnected from the main crack front (Fig. 3d).

For the post-mortem EBSD analysis of the sample (# 7 in the experimental procedure) the sample was cut along the plane depicted in Fig. 3a in order to analyse the grain orientations in this particular section of the sample. This study revealed that the planar portions of the crack are close (within 10°) to crystallographic {111} planes.

A better understanding of the crack morphology can be obtained when looking directly at a three dimensional representation of the crack surface. However because of the dual phase microstructure of the material (aluminium matrix plus silicon particles) this 3D representation is not straightforward. Indeed, in the reconstructed images, the gray levels of voxels corresponding to the crack and to the Si particles are both lower than the gray levels of voxels corresponding to the Al matrix; a mere segmentation based on gray levels would therefore extract the crack and the particles simultaneously. To avoid this problem, a sequence of 3D morphological filter operations [31] has been used and allowed the selective extraction of the crack surface from the 3D tomographic data. The result of this operation is illustrated on Fig. 3b and d for the

two slices described previously. It can be seen that the binary image, although slightly less accurate than the initial one, still provides a good description of the crack. It is thus possible to obtain a 3D rendering of the binary data set representing the crack. Such a rendering is shown on Fig. 4 where the crack surface intersection, examined in EBSD and optical microscopy is indicated by an arrow. A close examination of this figure reveals that, in fact, the apparently unconnected crack segments described in Fig. 3c do belong to the crack front.⁶ This illustrates clearly the difficulty of studying crack propagation from simple 2D observations. In the central part of the crack front (label #2), one can also distinguish the bifurcation number 3 shown previously in Fig. 3a. One striking feature of this 3D view is that the crack front does not appear as a regular circular line. It is rather formed by three independent main segments (labelled 1, 2 and 3) around 200 μm in length separated by uncracked Al matrix invisible in this rendering. This suggests that the crack front propagates first

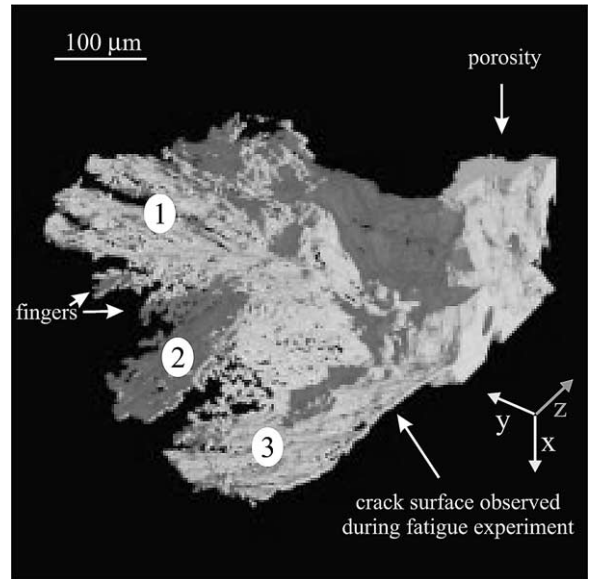


Fig. 4. Three dimensional rendering of the crack surface. Note the abrupt change in inclination of the central arc-shaped crack segment (#2). The finger-like crack extensions (see arrows) correspond to the crack fragments depicted in Fig. 3d.

⁶ Details labeled “finger” in Fig. 4.

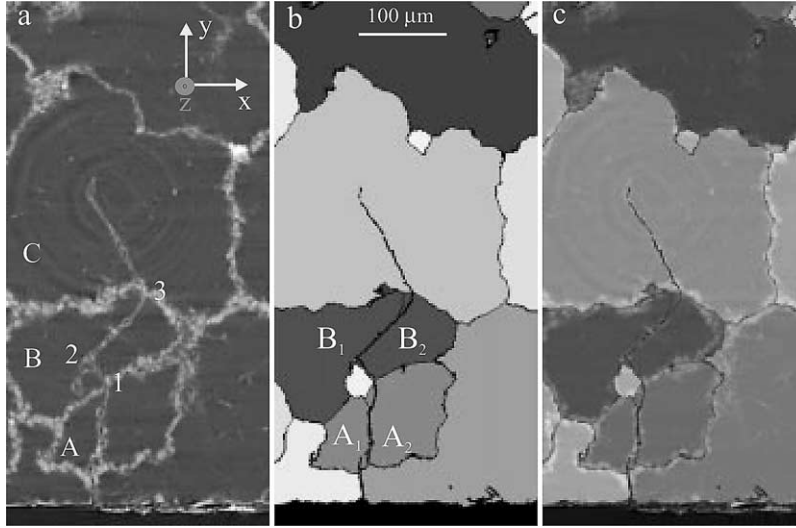


Fig. 5. a) Tomographic reconstruction after application of Ga. The depicted slice corresponds to the same section shown in Fig. 3a (energy: 15 keV, distance: 5 mm). b) Result of 3D morphologic segmentation: each cell detected by the segmentation algorithm receives a distinct label, represented here by different colours. Cells belonging to the same grain (A_1 & A_2 and B_1 & B_2) have been attributed identical colours. c) The superposition of the tomographic and the segmented data set shows a good agreement between both representations.

in “easy” zones of the crystal which might be grains showing favourable crystallographic orientations. In order to check this assumption we can now use the information about the 3D shape of the grains along the crack path.

3.3. Correlation between the crack shape and the internal grain distribution along the crack front

A first approach for studying the relation between the grain distribution and the crack morphology is to look at 2D reconstructed slices obtained after the wetting of the metal by gallium. Fig. 5a shows the identical section like Fig. 3a after application of the liquid metal. It appears that two of the abrupt changes in the crack propagation (1 & 3) are related to the passage of the crack into a new grain. Close to label 1 the crack deviates by $\approx 45^\circ$ when crossing the grain boundary between grains A and B. Then, for unknown reasons, the crack deviates by $\approx 90^\circ$ in the center of grain B. Finally, when crossing the grain boundary between grains B and C the crack deviates again by $\approx 75^\circ$.

Thanks to the 3D nature of our observations, it

is possible to study how the crack goes from grain B into grain C all along the crack front by simply looking at the different slices parallel to the XY planes. However, as discussed previously, this is better achieved by considering directly 3D images of the grains.

3D grain images have been obtained from the initial 3D data by morphological segmentation of the data set (see section 2.2). Fig. 5 illustrates the transformation of the tomographic reconstruction into the segmented and labelled representation. It can be seen that the grain boundary structure after segmentation (Fig. 5b) is in good agreement with the tomographic raw data: all grains have been detected and only a few inaccuracies can be observed (e.g. the additional small grain in the lower part, arising from over-segmentation). As already mentioned, gallium also wets the crack surface. Thus, when the crack is transgranular, the corresponding grain is split in two distinct cells by the segmentation algorithm. In that case, parts belonging to the same grain were attributed identical colours (in the 3D images), but still exist as distinct cells (see for example cells A_1 and A_2 in Fig. 5b) in the numerical representation of the data

set. Both data sets, the one containing only the crack and the labelled one containing the grains, were carefully aligned with respect to each other and finally merged for a simultaneous 3D visualization of both the crack and the grains. An example of such a visualization is shown in Fig. 6 which represents the 3D shape of two of the grains observed by EBSD in Fig. 2b. For a direct comparison the grains have been assigned the same colors in the EBSD map and in the 3D image. Part of grain G2 has been set transparent in the visualization: the smooth surface on the right side corresponds to a tomographic section close to the sample surface observed by optical microscopy and the rather rough surface (nearly parallel to the YZ plane) corresponds to one crack face in the grain.

It is interesting to note that the point Y^7 corresponds well to the position, where the sub-surface crack front (illustrated schematically by the black lines in Fig. 6a) had to cross a section of the grain boundary lying parallel to the crack front. A possible interpretation of this observation is given at the end of section 4.1.

The bifurcation number 3 on Fig. 5a can also be studied with the help of the 3D rendering of the grains. The results of the analysis are shown in Figs. 7 and 8. The first figure shows the 3D shape of the grain which is responsible for the crack bifurcation. It appears (Fig. 8a and b) that the crack enters a new grain (the one depicted in Fig. 7) along the curved lined A A". This line can be further divided in two sections: a first section AA' corresponding to a large advance ($\cong 100 \mu\text{m}$) of the crack in the grain by tilting around an axis which is roughly the intersection of the crack front with the boundary of the grain; and a second section A'A'' corresponding to a much smaller advance of the crack ($\cong 10\text{--}20 \mu\text{m}$) in the new grain by twisting of the crack front. A possible explanation of the preferential advance of the crack along A–A' might be given in terms of a continuity condition for the crack surface, as discussed in section 4.2.

4. Discussion

To the best of our knowledge, this is the first time that a simultaneous 3D image of a short fatigue crack and of the surrounding crystallographic grains has been obtained. The combination of the 3D tomographic measurements with conventional 2D surface observations (crack growth history and EBSD mapping) provides interesting information about various aspects of the interaction of short fatigue cracks with the grain structure in polycrystalline material.

4.1. Crack arrest at grain boundaries

One may distinguish two types of models describing the influence of the grain structure on fatigue crack propagation in polycrystals:

1. Models based on the varying elastic properties between neighboring grains.
2. Models based on the dislocation mechanisms and crystal plasticity ahead of the crack tip.

Representative for the first class of models we consider here recent work by Ravichandran and Li

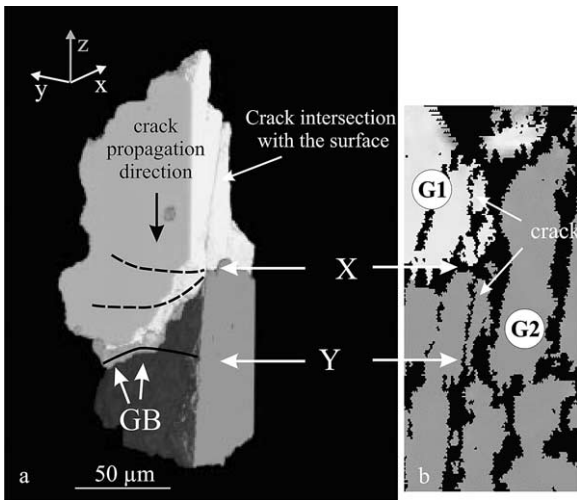


Fig. 6. a) 3D rendering of the local grain structure close to the crack stops observed at the sample surface at points X and Y. Both stops might be attributed to the pinning of the crack front at the grain boundary between grains G1 and G2. b) EBSD mapping of the corresponding sample area.

⁷ Retardation of surface crack propagation for about 20,000 cycles.

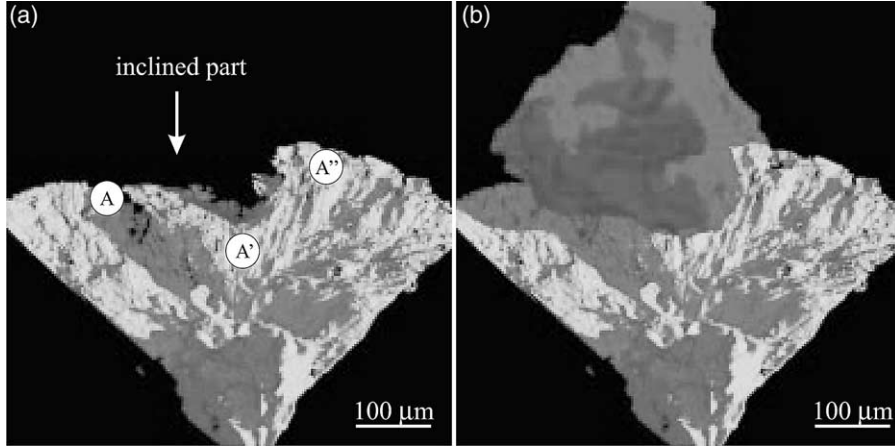


Fig. 7. The abrupt deviation in the crack propagation direction coincides with the transition into a new grain. a) Volume rendering of the crack surface as in Fig. 3 but from a different viewpoint. b) Rendering of the crack surface and the grain that caused the sudden deviation.

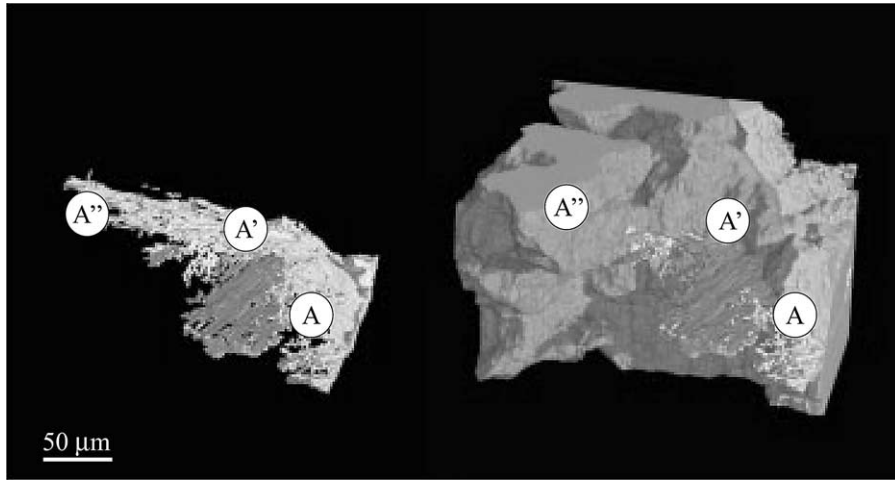


Fig. 8. a) 3D rendering of the crack inside the new grain (set to transparent). b) same scene with the surrounding grains. The crack entered the new grain between points A and A' by tilting. Between points A' and A'' the crack followed the contour of the grain. It is likely that the preferential attack along A–A' is governed by compatibility with favorable crystallographic orientations inside the grain.

[33] which accounts for the influence of the varying elastic modulus in the grains due to the change in grain orientation. Assuming isostrain conditions, these authors have established a method to calculate the local values of the stress intensity factor K along a crack front in heterogeneously stressed material and their model predicts strong variations of the local K values in the case of microstructural short cracks.

In order to test the applicability of this model, we calculated the elastic modulus of the surface grains along the loading direction, using the EBSD mapping and the relationship [34]

$$E = \left(s_{11} - 2 \left(s_{11} - s_{12} - \frac{s_{44}}{2} \right) (l_1^2 l_2^2 + l_2^2 l_3^2 + l_3^2 l_1^2) \right)^{-1} \quad (1)$$

where the terms s_{ij} correspond to the elastic constants of Al and l_i to the coordinates of the loading direction, expressed in terms of the vectors of the unit cell. The results are summarized in Table 2.

Due to the weak coefficient of anisotropy ⁸ of Al (1.2 compared to 2.5 in the case of Fe [35]) the elastic moduli show only moderate variations (7% with respect to the mean value) and the above mentioned mechanism is not expected to play a dominant role. Indeed, two of the crack stops observed at the sample surface (points *X* and *Z*) occur at the transition from a grain of low modulus into a grain of high elastic modulus, whereas one would expect the opposite behavior (acceleration rather than retardation) of the crack propagation rate in this situation.

This, together with the experimental evidence of localized plasticity ahead of the crack tip [14] seems to indicate that the second class of mechanisms plays a preponderant role in the present case. The common point of these mechanisms is the postulate that some plasticity has to be initiated in the new grain before the crack can enter it [7,8,5]. As a result the “waiting time” in the grain boundary should be a function of the misorientation between the two grains. Such stops are likely to happen frequently along the crack front, when the crack is small.

The quantitative analysis of the crack propagation data (i.e. the observed crack arrests at grain boundaries) in terms of such a dislocation based model, taking into account the local differences in the activation of the crystallographic slip systems, is under progress and will be reported elsewhere.

Irrespective of the underlying mechanism, the restriction of the observation of crack propagation on the sample surface may lead to erroneous

interpretation of the growth kinetics as the three-dimensional nature of the crack is neglected. There is experimental evidence that significant changes in the aspect ratio $2c/a$ (c surface length of the crack, a bulk length) may occur during the growth of short cracks [36]. The ideal characterization procedure should therefore include the continuous monitoring of the 3D crack shape during the fatigue experiment and the determination of the grain orientations in the bulk of the polycrystalline sample. The former task can be achieved by repeated microtomographic inspection during an interrupted fatigue test and the latter task can be performed with the help of a new non-destructive, synchrotron based diffraction technique [28,29].

For the current study we do not dispose over such detailed information on the crack growth history in the bulk of the sample. Nevertheless it is interesting to note that the crack retardation observed at point *Y* on the sample surface corresponds well to the position where the sub-surface segment of the crack has to pass a section of the grain boundary which lies parallel to the crack front. A possible interpretation of the retardation at point *Y* can therefore be given in terms of a crack arrest below the sample surface, which in turn influences the crack growth at the surface. The dashed lines in Fig. 6 have been added to illustrate the possible evolution of the crack front according to the above mentioned scenario.

4.2. Tilt and twist

The 3D tomographic reconstruction gives direct access to geometrical and morphological parameters of the crack surface in the bulk of the sample. This allows us, for example, to determine in a quantitative way the mixed-mode character of short cracks which often consist of several segments growing in different directions with respect to the loading axis. Coupled with in situ monitoring of the crack growth during the fatigue experiment, this information could be used in the future to assess the growth kinetics in a full fracture mechanical context, for example, by including the effect of crack deflections on the stress intensity factor [37].

However, interesting information can also be

Table 2
Elastic moduli along the loading direction, determined from the EBSD mapping (Fig. 2b) via relation 1

grain	G1	G2	G3	G4
modulus	63 GPa	67 GPa	67 GPa	72 GPa

⁸ Defined as the ratio of the elastic constants $2c_{44}/c_{11}-c_{12}$.

obtained from the analysis of the 3D crack morphology at a given state during fatigue life, i.e. without the knowledge of the crack history. The investigated crack consists of three segments with preferred growth directions. The analysis of the strongly inclined central segment with respect to the surrounding grain structure clearly revealed that the deflection of the crack is related to the passage of the crack into a new grain (Figs. 7 and 8).

Two factors are to be taken into account for the propagation of the crack. The first one is the activation of some plasticity on a crystallographic well orientated plane in the next grain. Our observations show that in the studied case the crack plane is close to a $\{111\}$ plane. The second factor that has to be considered is the geometry of the crack surface itself. It has been shown recently [21] by EBSD surface observations of an Al-Li alloy that short fatigue cracks growing on crystallographic planes tend to propagate by tilting rather than twisting of the crack front.

The reason for this is illustrated schematically in Fig. 9. The propagation of the crack by simple tilt of the crack front is more favorable, in terms of energy, than a propagation by twist. In the second case, indeed, the fracture surface is larger.

Our observations of the crack penetrating the grain depicted in Fig. 7 are in favor of this mechanism: the propagation of the crack in this grain is larger in the region where it can be accommodated by simple tilt (line AA' on Fig. 8). On the contrary, the grain resists propagation when it is

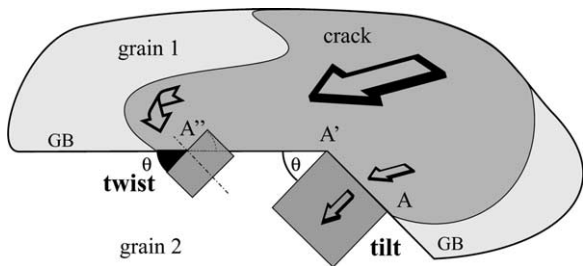


Fig. 9. The adaptation of a crack to a new plane may involve tilting and twisting. Note that twisting requires the creation of additional surfaces (black) in order to preserve the connectivity of the crack surface.

accompanied by a twist of the crack front (between A' and A'').

The observation of significant changes in the growth directions of cracks in the same material by conventional post mortem fractographic analysis (Fig. 10) gives additional support for the above mentioned mechanism: rather than homogeneous propagation into all grains close to the crack tip, the crack seems to follow the perimeter of some of the grains until propagation into these grain starts in a lateral direction.

It should be emphasized that the analysis of a larger number of fatigue cracks, including the crystallographic characterization of the adjacent grains, is necessary to corroborate the validity of this tilting/twisting mechanism.

5. Conclusions

This paper presents a new technique for the simultaneous three-dimensional visualization of fatigue cracks together with the surrounding grain structure in the bulk of polycrystalline Al samples. Penetration of liquid Ga along the Al grain boundaries leads to the formation of microscopic wetting

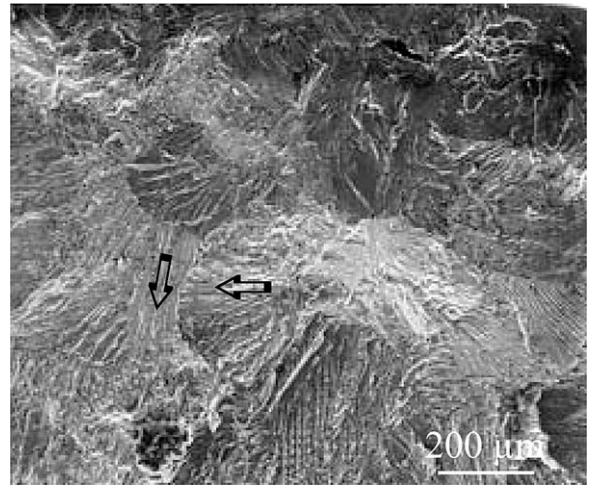


Fig. 10. SEM micrograph of the fracture surface of a sample tested at 120 MPa ($N_R=2075200$). The characteristic crack growth patterns indicate significant changes in the propagation direction of the crack.

layers which in turn can be detected by high resolution X-ray absorption tomography.

The studied short fatigue crack appears to consist of three crack segments corresponding to the crack growth in different grains. The stop and go motion of the crack, observed by optical microscopy at the sample surface, is clearly related to the grain structure directly at and close to the sample surface. The tentative interpretation of these crack stops in terms of an elastic model supposing isostrain conditions fails, presumably due to the weak coefficient of anisotropy of Al. The three-dimensional analysis of the crack with respect to the grain structure indicates that the passage of the crack into a new grain occurs preferentially from regions on the grain perimeter, where the growth can be accommodated by tilting of the crack plane. On the contrary, the crack has difficulties in entering the new grain from regions where twisting of the crack plane is required and tends to grow along the grain perimeter.

Future experiments should include repeated microtomographic characterization of the 3D crack shape during (interrupted) fatigue tests. This, together with the characterization of the grain orientation in the bulk of the material via modern synchrotron diffraction techniques will provide the necessary information to assess the problem of fatigue crack propagation in terms of a full three-dimensional fracture mechanical context and to analyse the physical mechanisms governing crack propagation.

Acknowledgements

We would like to thank P.H. Jouneau (INSA Lyon) and P. Buffat (CIME, Lausanne) for the EBSD characterization. We are also much indebted to D. Jeulin and S. Bouchet (Ecole des Mines, Paris) who provided and implemented the 3D image segmentation routines. D. Bellet and Y. Brechet (INPG, Grenoble) are acknowledged for useful discussions on various aspects of the work.

References

- [1] Miller KJ. The short crack problem. *Fatigue Eng Mater Struct* 1982;5(3):223–32.
- [2] Miller KJ, de los Rios ER. *The behaviour of short fatigue cracks*. London: European Group of Fracture, 1986.
- [3] Suresh S. *Fatigue of materials* 1st ed. Cambridge: Cambridge University Press, 1994.
- [4] Zurek AK, James MR, Morris WL. The effect of grain size on fatigue growth of short cracks. *Metall Trans A* 1983;14:1697–705.
- [5] Lankford J. The growth of small fatigue cracks in 7075-T6 aluminium. *Fatigue Fract Eng Mater* 1982;5(3):233–48.
- [6] Lankford J. The influence of microstructure on the growth of small fatigue cracks. *Fatigue Eng Mater Struct* 1985;8(2):161–75.
- [7] Zhang YH, Edwards L. Measurement of plastic zones associated with small fatigue cracks by selected area channeling patterns. *Mater Charac* 1992;29:313–20.
- [8] Turnbull A, de los Rios ER. The effect of grain size on the fatigue of commercially pure aluminium. *Fatigue Fract Eng Mater* 1995;18(12):1455–67.
- [9] Turnbull A, de los Rios ER. The effect of grain size on fatigue crack growth in aluminium magnesium alloy. *Fatigue Fract Eng Mater* 1995;18(11):1355–66.
- [10] Clement P, Angeli JP, Pineau A. Short crack behaviour in nodular cast iron. *Fatigue Eng Mater Struct* 1984;7(4):251–65.
- [11] Tokaji K, Ogawa T, Harada Y, Ando A. Limitations of linear elastic fracture mechanics in respect of small fatigue cracks and microstructure. *Fatigue Fract Eng Mater* 1986;9:1–14.
- [12] Guvelenir A, Breunig TM, Kinney JH, Stock SR. Direct observation of crack opening as a function of applied load in the interior of a notched tensile sample of Al-Li 2090. *Acta Mater* 1987;45(5):1977–87.
- [13] Buffière J-Y, Maire E, Lormand G, Fougères R. Characterisation of internal damage in a MMC_p using X-ray synchrotron phase contrast microtomography. *Acta Mater* 1999;47(5):1613–25.
- [14] Savelli, S. *Analyse des mécanismes et modélisation de la durée de vie en fatigue d'alliages de moulage AS7G03*. PhD thesis, INSA Lyon, May 2000.
- [15] Martin CF, Josserond C, Salvo L, Blandin J-J, Cloetens P, Boller E. Characterisation by X-ray micro-tomography of cavity coalescence during superplastic deformation. *Scr Mater* 2000;42:375–81.
- [16] Babout L, Maire E, Buffière J-Y, Fougères R. Characterization by X-ray computed tomography of decohesion, porosity growth and coalescence in model metal matrix composites. *Acta Mater* 2000;49:2055–63.
- [17] Maire E, Owen A, Buffière J-Y, Withers PJ. A synchrotron X-ray study of a TiSiC_f composite during in situ straining. *Acta Mater* 2001;49:153–63.
- [18] Everett RK, Simmonds KE, Geltmacher AB. Spatial distri-

- bution of voids in HY-100 steel by X-ray tomography. *Scr Mater* 2001;44:165–9.
- [19] Cloetens P, Pateyron-Salomé M, Buffière J-Y, Peix G, Baruchel J, Peyrin F. Observation of microstructure and damage in materials by phase sensitive radiography. *J Appl Phys* 1997;81(9):5878.
- [20] Ludwig W, Bellet D. Penetration of liquid gallium into the grain boundaries of aluminium: a synchrotron radiation microtomographic investigation. *Mat Sci Eng A* 2000;281:198–203.
- [21] Zhai T, Wilkinson AJ, Martin JW. A crystallographic mechanism for fatigue crack propagation through grain boundaries. *Acta Mater* 2000;48:4917–27.
- [22] Buffière J-Y, Savelli S, Jouneau PH, Maire E, Fougères R. Experimental study of porosity and its relation to fatigue mechanisms of model Al-Si7-MgO.3 cast Al alloys. *Mat Sci Eng A* 2001;A 316:115–26.
- [23] Koch, F. Peyrin, P. Heurtier, B. Ferrand, B. Chambaz, W. Ludwig, and M. Couchaud. X-ray camera for computed microtomography of biological samples with micrometer resolution using $\text{Lu}_3\text{Al}_5\text{O}_{12}$ and $\text{Y}_3\text{Al}_5\text{O}_{12}$ scintillators. *Proc. SPIE*, 3659:170-178, 1999.
- [24] Labiche, JC., Segura-Puchades, J., Van Brussel, D., Moy, JP. FRELON camera: Fast REadout LOw Noise. *ESRF Newsletter*, 25, 1996.
- [25] Morawe C, Pecci P, Peffen JC, Ziegler E. Design and performance of graded multilayers as focusing elements for X-ray optics. *Rev Sci Instrum* 1999;70:3227–32.
- [26] Kak AC, Slaney M. Principles of computerized tomographic imaging. New York: IEEE Press, 1988.
- [27] Inkson BJ, Mullvihill M, Möbus G. 3D determination of grain shape in a FeAl-based nanocomposite by 3D FIB tomography. *Scr Mater* 2001;45:753–8.
- [28] Poulsen HF, Nielsen SF, Lauridsen EM, Schmidt S, Suter RM, Lienert U, Margulies L, Lorentzen T, Juul Jensen D. Three-dimensional maps of grain boundaries and the stress-state of individual grains. *J Appl Cryst* 2001;34:751–6.
- [29] Lauridsen EM, Schmidt S, Suter RM, Poulsen HF. Tracking: a method for structural characterization of grains in powders or polycrystals. *J Appl Cryst* 2001;34:744–50.
- [30] Ludwig, W. Development and Applications of synchrotron radiation microtomography. PhD thesis, Ludwigs-Maximilians Universität München, 2001.
- [31] Gratin C, Meyer F. Mathematical morphology in three dimensions. *Acta Stereologica Suppl I* 1992;11:551–8.
- [32] Meyer F. Mathematical morphology: from two dimensions to three dimensions. *J Microsc* 1992;165(1):5–28.
- [33] Ravichandran KS, Li X-D. Fracture mechanical character of small cracks in polycrystalline materials: Concept and numerical k calculations. *Acta Mater* 2000;48:525–40.
- [34] Nye JF. Physical properties of crystals. Oxford: Oxford University Press, 1985.
- [35] Cottrell AH. The mechanical properties of matter. John Wiley and Sons, 1964.
- [36] Ravichandran KS. Three-dimensional crack-shape effects during the growth of small surface cracks under fatigue in a titanium-base alloy. *Fatigue Eng Mater Struct* 1997;20:1423.
- [37] Suresh S. Crack deflection: Implications for the growth of long and short fatigue cracks. *Metall Trans A* 1983;14:2375–85.